THE ASTROPHYSICAL JOURNAL, 275:445–460, 1983 December 15

BROAD EMISSION FEATURES IN QSOs AND ACTIVE GALACTIC NUCLEI. I. NEW CALCULATIONS OF Fe II LINE STRENGTHS

HAGAI NETZER
Department of Physics and Astronomy and the Wise Observatory, Tel Aviv University
AND
BEVERLEY J. WILLS
Department of Astronomy and McDonald Observatory, University of Texas at Austin
Received 1983 February 8; accepted 1983 May 13

ABSTRACT

This is the first of two papers investigating the problem of some broad emission features in the spectra of quasars and Seyfert galaxies. Fe II lines are thought to contribute to these features, and in this first paper we discuss their formation within the general framework of photoionization models. We treat many more lines (1926) and multiplets (608) than in previous work, and we show that this results in significant changes in the calculated spectrum. We find: (1) Wavelength coincidences of different Fe II lines cause pumping and excitation of many high energy ($E \geq 7$ eV) levels. Lines arising from these levels are strong and this fluorescence effect largely explains the previous poor agreement between the calculated and observed Fe II spectrum. Fluorescence with Mg II λ2802.7 is marginally important, and there is a small contribution from absorption of C IV λ1549. (2) Radiative excitation via absorption of continuum photons contributes significantly ($\sim$10%) to the emergent flux, mainly in the ultraviolet. (3) The relative strengths of the ultraviolet and optical Fe II bands depend on the optical depth and turbulent velocity. Large optical depth is required to produce strong optical Fe II lines, but strong ultraviolet Fe II emission may be common in many, small optical depth objects. We demonstrate that the 3000–3500 Å Fe II feature is a potentially useful tool in analyzing the spectrum of weak optical Fe II objects. (4) Fe II line fluorescence is also important in emission in late-type stars and possibly in other astronomical objects. Detailed comparison of our calculations and the observed spectrum of the emission star RR Tel provide confirmation of the general correctness of our model, including the approximations used for collision strengths and the effects of line fluorescence.

Subject headings: galaxies: nuclei — galaxies: Seyfert — line formation — quasars — stars: emission-line — stars: individual

I. INTRODUCTION

Fe II lines in Seyfert galaxies and quasars have been the subject of many papers since their first discovery by Wampler and Oke (1967). The theoretical and observational aspects of this problem have been addressed by Osterbrock (1977), Phillips (1978*a*, *b*), Collin-Souffrin *et al.* (1979), Joly (1981), and others. The line excitation mechanism was suggested to be either absorption of continuum photons or collisional excitation (see the review by Davidson and Netzer 1979).

We have contributed to the study of this problem in three papers: Netzer (1980, hereafter Paper I) argued that collisional excitation of Fe^+, within the framework of photoionization models, is the dominant mechanism for producing these lines in quasars and Seyfert galaxies. Wills *et al.* (1980, hereafter Paper II) gave the first evidence for strong ultraviolet Fe II lines in many quasars. Later, Wills, Netzer, and Wills (1981, hereafter Paper III) discussed several weak unidentified emission features in quasar spectra and argued that they are Fe II lines arising from high energy ($E \gtrsim 8$ eV) levels.

Although collisional excitation is quite successful in explaining the total emergent flux in Fe II lines, there are still large discrepancies between the calculated and observed strength of individual features. Our previous model (Paper I) and others (e.g., Kwan and Krolik 1981; Joly 1981) cannot produce the observed shape of many ultraviolet Fe II blends. In particular, several high energy transitions are observed to be much stronger than predicted in standard models, where the electron temperature is too low to excite them ($T \lesssim 10^4$ K). (We noted this difficulty in Paper III.)

Recent work by Grandi (1981) emphasized this problem even more strongly. By careful fitting of the spectrum from 2000 to 5000 Å, he was able to show that there are many "gaps" in the theoretical spectrum that

can only be filled in by high energy Fe II transitions. He then proceeded to fit the observations by assuming, without justification, that these high energy transitions are indeed very strong. Clavel (1983) and Puetter (1983) have noted this, too. The same problem arises in other astronomical objects. For example, strong high energy transitions are observed in the spectrum of symbiotic stars (Penston *et al.* 1983; Nussbaumer and Schild 1981), late-type stars (van der Hucht *et al.* 1978), and Eta Carinae (Johansson 1977).

In this paper and a later one, we present new calculations of Fe II line strengths, taking into account processes that were not considered previously. This paper concentrates on the theoretical aspects of the problem, and on ways to explain the energy output in the high energy transitions. In the second paper we use these results to fit new observations of quasars and active galaxies.

II. CALCULATIONS

a) General Considerations

We wish to calculate the relative strengths of a large number of permitted Fe II lines arising from excited, odd-parity, levels of energies up to 9.1 eV. Numerous even-parity levels have, on the average, lower energies, and we include those with $E \leq 7.5$ eV in our scheme. Since the atomic data are poorly known and the treatment of line transfer very complicated, we look for general properties to simplify the problem. The method used is similar to the one employed in Paper I, but modified to include many more transitions. We briefly outline its main points.

It is easy to show that under LTE, and for transitions with $h\nu \gg kT$, the emission line intensities $I(\lambda)$, are given by

$$I(\lambda) \propto \frac{1}{\lambda^4} e^{-h\nu/kT}. \quad (1)$$

Moreover, this relation gives a fairly good approximation to the line intensities under more general conditions where only some of the levels are populated in their Boltzmann ratios. To see this, consider the transition (i, j), where i and j indicate the lower and upper levels and a point in the cloud where the optical depth to the surface, in a given direction, is τ_{ij}. We associate with this optical depth a local escape probability, ε_{ij}, given by

$$\varepsilon_{ij} = \frac{1 - e^{-\tau_{ij}}}{\tau_{ij}}. \quad (2)$$

This dependence on optical depth is a good approximation for both large and small τ_{ij} in most cases of interest (Ferland and Netzer 1979, and references therein). For a thermal absorption profile

$$\tau_{ij} \propto N_i f_{ij} \lambda_{ij} \propto \lambda_{ij}^3 A_{ji} N_i \frac{g_j}{g_i}, \quad (3)$$

where g_i and g_j are the statistical weights of the levels and other symbols have their usual meanings. Using relationships (2) and (3) we get

$$I(\lambda_{ij}) = N_j A_{ji} \varepsilon_{ij} h\nu_{ij} \propto \frac{1 - e^{-\tau_{ij}}}{\lambda_{ij}^4} \frac{(g_i/N_i)}{(g_j/N_j)}, \quad (4)$$

which reduces to equation (1) in the limit of large τ_{ij} and Boltzmann distribution of level population.

The relative intensity of transitions with a *common* upper level, j, and different lower levels in thermal equilibrium, i, is proportional to

$$\frac{1 - e^{-\tau_{ij}}}{\lambda_{ij}^4} e^{E_i/kT}, \quad (5)$$

where E_i is the energy of level i. Relative intensities of such lines are in their LTE values for large enough optical depth, despite the fact that the common upper level may not be thermally populated.

The above argument was used in Paper I (eqs. [5]–[8] there) to compare the relative strengths of optical and UV Fe II multiplets with a common upper level. It enables us to predict the intensities of many lines since many of the lower, even-parity levels of the Fe^+ atom are indeed in thermal equilibrium under the conditions of temperature and high density in quasar broad emission-line clouds.

Equations (1)–(5) are particularly useful in estimating the relative intensities of lines within one multiplet. In this case we make the further assumption that all levels within a given term are populated according to their statistical weights (a very good assumption for most even-parity terms, but perhaps not as good for the odd-parity ones; see discussion later). Assume N_u atoms in the upper term and N_d in the lower one, then $N_j = N_u g_j / \Sigma g_j$ and $N_i = N_d g_i / \Sigma g_i$. Substitution into expression (4) shows that relative line intensities, within a multiplet, are again proportional to $(1 - e^{-\tau_{ij}})/\lambda_{ij}^4$. This, and the fact that energy separation within a term is negligible, enables us to reduce the number of levels in the calculations and still retain individual line intensities.

In the following calculations we assume that the line intensities within a multiplet are proportional to $(1 - e^{-\tau_{ij}})/\lambda_{ij}^4$. In several places we comment on the possible risks in using this simplified assumption.

b) Method

In our computation we consider 70 terms of the Fe^+ atom and the corresponding 608 permitted multiplets (1926 lines). We consider all the even-parity levels (32 terms) in Johansson's (1978*a*) tables, up to an energy of 7.5 eV, and assume that they are in thermal equilibrium, a good assumption for the range of densities considered

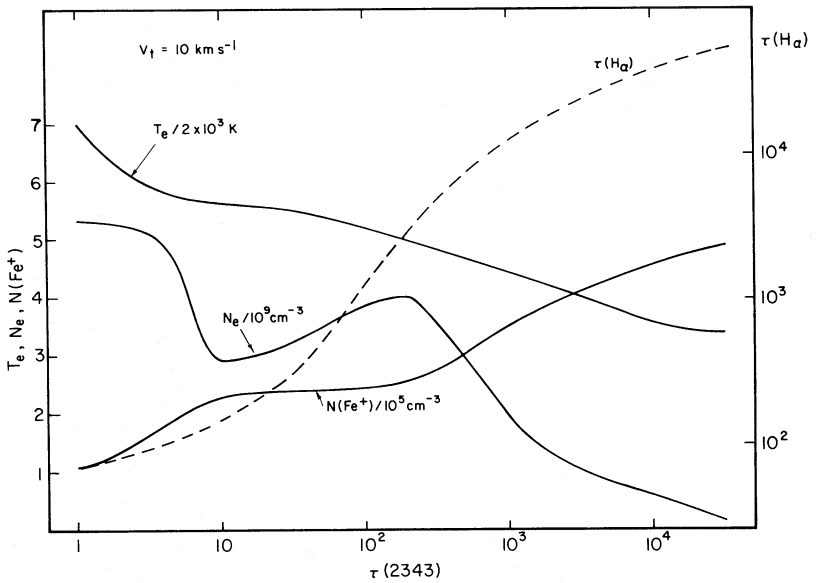

FIG. 1.—The run of density temperature Fe^+ abundance and $\tau(H\alpha)$ across a cloud in the standard model. $F_\nu = c\nu^{-0.4}\exp(-\nu/90$ ryd), $U_1 = 1.2\times10^8$ cm s^{-1} and cosmic abundances. V_t is the turbulent velocity in the cloud. Cases of different V_t than the one shown can be obtained by noting that $\tau(2343)\times V_t = const.$

(10^8–10^{10} cm^{-3}); see, however, § II*c* below. This simplifies the problem considerably. The remaining 38 terms include all the odd-parity levels in the Johansson list, with energy up to 9.1 eV. (Note that several odd-parity levels are as low as 4.8 eV—at lower energies than some of the so-called low even-parity levels.) The number of multiplets and lines in our program far exceeds that in the Moore (1945, 1950) multiplet tables, and many of them are taken from the Kurucz (1981) and Johansson (1978*a*) lists.

We assume a plane-parallel gas cloud divided into 200 layers in optical depth space, where the variable parameter is $\tau(2343)$, the optical depth in the strongest UV3 line. The division is such that the optical depth in layers close to the inner, illuminated face of the cloud is much smaller than in the outer layers. This improves the treatment of line transfer, since most line excitation takes place where the optical depth is lower and the temperature higher. In each layer we solve the equation of statistical equilibrium for all levels, using a *local escape probability* in the lines and assuming that half the photons are emitted inward (toward the central source) and the other half outward. For the escape probability we take

$$\varepsilon(\tau) = \begin{cases} \dfrac{1-e^{-\tau}}{\tau} & \tau \le e \\ \dfrac{1-e^{-\tau}}{\tau(\ln\tau)^{1/2}} & \tau > e. \end{cases} \quad (6)$$

This gives somewhat smaller values than equation (2) at large optical depths, in better agreement with radiative transfer calculations (e.g., Kwan and Krolik 1981, and references therein). The difference does not strongly affect the general conclusions reached earlier.

Photoionization calculations, as described in Paper I, are used to obtain the run of T_e, N_e, and $N(Fe^+)$ across the cloud. This is converted to a $\tau(2343) = f[T_e, N_e, N(Fe^+)]$ functional form and used to define $\tau(2343)$ for each layer. In each layer optical depths for all other Fe II lines are obtained by solving the even-parity level populations with the given T_e, N_e, $N(Fe^+)$ and assuming constant turbulent velocity throughout. The process is carried out twice; first to obtain the optical depth in all layers and all multiplets (i.e. the even-parity level population), and second to solve for the odd-parity level populations with these optical depths.

An example of a typical $[\tau(2343), N_e, T_e, N(Fe^+)]$ relation is shown in Figure 1. In this case $F_\nu \propto \nu^{-0.4}\exp(-\nu/90$ ryd) and the ionization parameter, $U_1 \equiv F_1/4\pi R^2 h N_e = 1.2\times10^8$ cm s^{-1}. (F_1 is the value of F_ν at 1 ryd.) We have calculated other models, with different power laws and U_1, and find that Figure 1 is typical of many cases with $10^8 \lesssim U_1 \lesssim 10^9$ cm s^{-1}, and $0.3 \le \alpha \le 1.5$. Generally speaking, a larger U_1 gives a larger optical depth at a given temperature, and flatter ionizing continua give higher temperatures for the same $\tau(2343)$. Since $\tau(2343)$, which is the most important factor in defining the relative strengths of Fe II lines (see § III), depends on both U_1 and the turbulent velocity, it is difficult to assess the value of U_1 from Fe II lines alone.

It is important to note that the Fe^+ column density is defined by the model, and the turbulent velocity, V_t, is

the only free parameter. For a given photoionization model and a thermal absorption profile $\tau(2343)\times V_t = const$, and changing one of them requires change in the other. In most cases of interest, there is no significant Fe II line emission beyond the point where the electron temperature has dropped to about 6000 K. Specifying a model by its $\tau(2343)$ therefore specifies the optical depth at that critical temperature for the chosen V_t.

Figure 1 also shows the Hα optical depth, $\tau(\mathrm{H}\alpha)$, which, over most of the Fe II line excitation zone, is proportional to $\tau(2343)$. This has important implications regarding the conditions in the low ionization zone, as will be discussed later.

c) *Atomic Data*

A known, yet unsolved, problem is the poorly known atomic data for the Fe^+ atom. This was discussed in Paper I and elsewhere (e.g., Joly 1981 and references therein). Despite recent progress (Nussbaumer and Storey 1980; Nussbaumer, Pettini, and Storey 1981; Moity 1983), there are still large uncertainties in collision strengths and f values. We have attempted to choose the best available data using Joly (1981), Phillips (1979), Moity (1983), Nussbaumer and Storey (1980), and Nussbaumer, Pettini, and Storey (1981) as our main sources. Those gf values that do not appear in Phillips (1979) or Moity (1983) were obtained from Kurucz (1981). Collision strengths are those given in Nussbaumer and Storey (1980), Nussbaumer, Pettini, and Storey (1981), or else estimated from

$$\Omega_{ij} = 4.5\times10^{-3}\Sigma\lambda gf(\text{multiplet}). \quad (7)$$

This relation predicts somewhat larger Ω_{ij} than those given in Paper I (eq. [10] there) and gives better agreement with most of Joly's (1981) Ω_{ij}s. We have introduced a lower limit of $\Omega_{ij} = 7$ for all transitions, to avoid unacceptably small Ω_{ij}/g_i. This is not unjustified as the computed collision strengths for some forbidden transitions among even-parity levels have Ω_{ij}/g_i larger than this limit (Nussbaumer and Storey 1980). We have also tried to keep $\Omega \propto \Sigma\lambda gf$ for all multiplets, even those with small Σgf. We achieve this by slight scaling of Ω_{ij} (in proportion to the calculated Σgf) near the minimum value of 7. The only exceptions to this scheme are several transitions leading from the lowest three even-parity terms (a^6D, a^4F, a^4D) to z^4D^o and z^4F^o. Using known gf values here would give Ω_{ij} near the minimum value of 7. However, it is clear from the inspection of quasar, Seyfert 1 galaxy, and symbiotic star spectra (Phillips 1978*a*; Thackeray 1977) that the above odd-parity levels give rise to some of the strongest observed multiplets (optical multiplets 37, 38, 48, 49, etc.). These terms must be highly populated and one possibility is that equation (7) underestimates their collision strengths. We have increased Ω_{ij} slightly in those transitions. As will be seen later, there are other, more important ways to increase the population of z^4D^o and z^4F^o, and our increasing of Ω_{ij} does not have a large effect on our final results. A full listing of the values of Ω_{ij} used is available upon request.

An important point to note is that our assumption of Boltzmann populations for all even-parity levels implies that collisional contributions to a given odd-parity level from different even-parity levels depend only on the value of Ω_{ij}. Neither the energy nor the statistical weight of the even-parity level enters the sum, provided its energy is lower than that of the odd-parity level. There are 32 even-parity terms in our scheme, and for most transitions $\Omega_{ij} \approx 7$ (typically two to six transitions out of the 32 contributing to a given upper term have $\Omega_{ij} \sim$ 30–100). The *summed* collisional contribution to all odd-parity levels with similar energy is therefore very much the same.

An important related issue is the collisional contribution to odd-parity levels from even-parity ones with *larger* energies (e.g., y^4P at ~ 7.5 eV to C^2F^o at ~ 5.5 eV) which, unlike transitions from lower lying levels, do not favor odd-parity levels with smaller energy. The collision strengths for such transitions are unknown, but the possibility that they are large and therefore important must be kept in mind. A further complication is that some low-energy odd-parity to high-energy even-parity transitions are optically permitted, and spontaneous decay is important. This reduces the population of the $E \gtrsim 6$ eV even-parity terms (six out of 32 in our scheme) to below their assumed Boltzmann populations. As will be shown in § II*e* below, these are not the dominant processes determining the level populations of Fe^+, and the neglect of such permitted transitions does not change much the nature of the problem.

Collisional transitions among odd-parity levels must also be considered. Three of the collision strengths for these are roughly known (Nussbaumer and Storey 1980) and are between 30 and 50. Without any better values, we have chosen $\Omega = 30$ for all the others. Within the range of densities, temperatures, and optical depths considered in our model, the exact values of Ω, within a factor of ~ 3, are not crucial.

Last, but not least, are collisional transitions among odd-parity levels *within* the same *term*. In our scheme such levels are assumed to be in thermal equilibrium, since this is the only way to include so many levels in the computation. This, however, is not a very good assumption, even in high density quasar clouds. The critical electron density, N_c, for this to be true is given roughly by:

$$\frac{8.63\times10^{-6}}{(T_e)^{1/2}} N_c \sum_i \frac{\Omega_{ij}}{g_j} > \sum_i A_{ji}\varepsilon_{ij} \approx \sum_i A_{ji}/\tau_{ij}. \quad (8)$$

Typically $A_{ji}/\tau_{ij} \sim 2\times10^3$, and there are about five

strong collisional transitions for each radiatively permitted one. Assuming $\Omega_{ij}/g_j \approx 2$, we get $N_c > 3\times10^{10}$ cm^{-3}. The above A_{ji}/τ_{ij} is calculated at the slab center and therefore gives the lowest limit for N_c. Total multiplet intensities calculated with the simplified statistical distribution assumption may not change much due to this, although the strengths of *individual lines* may. Other related difficulties are discussed in § II*e* below.

We do not know of any obvious way to improve the approximations described above and can only repeat the general warning that the poorly known atomic data of the Fe^+ atom is a major limitation in fitting models to observations.

d) *Absorption of Continuum Photons*

The absorption and reemission of continuum photons in resonance lines (sometimes called "the fluorescence mechanism") has been discussed by Osterbrock (1977), Phillips (1978*b*) and many others since, including Paper I, where it was found that the process could not contribute much to the observed lines. The argument was based on the narrow absorption profile and the small covering factor of the emission line clouds, $\Omega/4\pi$, which limits the number of absorbed continuum photons. However, only about 50 optically thick lines were considered there. In the present study we have considered many more transitions and have found more than 1000 optically thick lines. The process must therefore be reconsidered.

Assuming constant turbulent velocity, V_t km s^{-1}, throughout the gas, and a thermal profile, we can calculate the total absorption equivalent width, W(total), in the standard way. Using our computer code we find for it the following empirical relation:

$$W(\text{total}) \approx 350\left(\frac{V_t}{10}\ \text{km s}^{-1}\right)\left[\frac{\tau(2343)}{10^4}\right]^{0.2}\ \text{Å} \quad (9)$$

for $10^3 \lesssim \tau(2343) \lesssim 10^5$ and no line overlapping. [The reason for the deviation from the expected $(\ln\tau)^{1/2}$ dependence in eq. (9) is the contribution of many small optical depth lines to W(total).] Taking a covering factor of 0.1 and $V_t \approx 5$ km s^{-1}, we get that the emission equivalent width, due to the reemission of the absorbed flux, is $\approx$17 Å, which is about 10% of the observed value (Paper II). Line overlapping reduces this somewhat, but more realistic absorption profiles tend to increase it.

Another way to view this is to consider the 2000–3000 Å range, where most of the strong optically thick lines appear. For sufficiently large V_t, most of the energy in that wavelength range will be absorbed from the continuum, and the resulting emission equivalent width can approach the observed value of about 100 Å. Phillips's (1978*b*) and Osterbrock's (1977) original calculations of continuum fluorescence discussed this possibility, assuming very broad ($V_t > 100$ km s^{-1}) absorption profiles. This is not needed when all the known Fe II transitions are included. In such a case $V_t \approx 20$–40 km s^{-1} is large enough to absorb most of the 2000–3000 Å continuum.

Even if continuum absorption is not significant in adding to the intensity of the strongest lines, it may well be an important factor in contributing to some weak features. We mentioned this possibility in Paper III, but the implication of having such a large number of optically thick transitions was not fully appreciated then.

In the following calculations we assume a nonthermal continuum source and allow for absorption of continuum photons in all permitted lines. This extra contribution is considered locally, for all layers, according to the optical depth at that location. We assure self-consistency by assuming a covering factor (typically $\Omega/4\pi \sim 0.1$) and demanding that the total emergent flux in the lines, including all processes, agrees with the observed emission equivalent width. Larger V_t implies smaller optical depth in the lines, since the emitted flux, and therefore the column density of Fe^+ atoms, is fixed by self-consistency requirement. This [$(V_t, \tau(2343))$] combination fixes the number of continuum photons absorbed in that model. $\tau(2343)$ and the optical depth in other transitions originating form the a^6D and a^4F ground terms can reach very large values, but mostly in the low T_e, low N_e outer regions, which do not contribute appreciably to collisional excitation. The optical depth for transitions originating from higher energy levels, quickly approaches a terminal value, due to the drop in temperature.

e) *Line Fluorescence*

As noted in Paper III and above, observations of quasars and Seyfert galaxies show evidence of lines arising from high energy levels, which cannot all be explained by collisional excitation at the low expected temperatures ($T_e \leq 10^4$ K). The same phenomenon is known in the spectrum of some emission nebulae and late-type stars (Johansson 1977; van der Hucht *et al.* 1978; Brown, Jordan, and Wilson 1979). Another good example of high level excitation is the UV spectrum of RR Tel (Penston *et al.* 1983) where many lines from levels with $E > 7$ eV are clearly observed. Obviously, some process other than radiative recombination or collisional excitation is required, and this process may also be operating in quasars.

A potentially important mechanism for exciting the Fe^+ high energy levels is line fluorescence, via wavelength coincidence with strong lines of other elements. The process was suggested by Gahm (1974) and was later discussed by van der Hucht *et al.* (1978), Brown, Jordan, and Wilson (1979), Penston *et al.* (1983), and others. Gahm's original work indicated that fluorescence with the strong Mg II doublet at 2795.528 and 2802.704

Å is most important for Fe II and other ions. Another possibility is fluorescence with hydrogen Lyman and Balmer lines.

There are two difficulties with this idea: first, Gahm's (1974) list includes line coincidence with wavelength separation of up to 100 km s^{-1}. This separation is more than an order of magnitude larger than the expected thermal width of the line considered, and the only way in which it can become important is if turbulent velocities, of that order of magnitude, are typical of the line emitting zone. Dynamically this is hard to accept, and, in addition, the optical depth in the Fe II transitions, and hence the fluorescence efficiency, will drop if the absorption profile is so wide. Restricting ourselves to lines within several thermal widths of each other, in Gahm's (1974) list, there are too few of them to explain the observed effect. Second, the work of Gahm (1974) and others is based on Fe II wavelengths listed in Moore (1945, 1950) tables. This reference is very incomplete and includes inaccurate line wavelengths. The recent compilation by Kurucz (1981), with wavelengths calculated from Johansson's (1978*a*) new energy levels, is a much better reference and should be used for rechecking the idea of wavelength coincidences.

We have used Kurucz's (1981) tabulation to check for wavelength coincidences of Fe II transitions with strong lines of other elements. Three conditions must be satisfied for this process to be efficient: (*i*) large enough optical depth in the Fe II transitions, (*ii*) wavelength differences to within several thermal widths (assuming no large turbulent velocity; see below) between the Fe II lines and those of the other elements, and (*iii*) the line formation zones of Fe II and the other element considered must overlap. Condition (*iii*) above is not absolutely essential, but it makes the fluorescence more efficient, since every scattering of the exciting photons increases the chance of their being absorbed by Fe^+. Most suitable, therefore, are lines of Mg II, O I, and H I.

Our search yielded several coincidences that are potentially important. Mg II λ2802.704 is 11.3 km s^{-1} away from a Fe II line at 2802.599 Å, which, in our model, can reach an optical depth of 1–10. Mg II λ2795.528 is 25.6 km s^{-1} away from another Fe II line, which we consider to be too far in wavelength separation for efficient fluorescence. Lyα λ1215.67 is 5.9 km s^{-1} away from an Fe II line, at 1215.694 Å, that can have, in our model, an optical depth of ~1. Another Fe II line at 1215.852 Å (44.9 km s^{-1} from Lyα line center) can reach an optical depth of 5–10 and may be of some importance considering the large optical depth expected in Lyα. Lyβ λ1025.722 is almost perfectly matched in wavelength with Fe II λ1025.725, which is expected to have optical depth of about 1. Of the strong lines formed in the high excitation H^+ zone we shall mention wavelength coincidences with C IV λ1548.185 (3.7 km s^{-1} away from an Fe II line with optical depth of ~ 7), N V λ1238.82 (1.2 km s^{-1} away from an Fe II line with optical depth of about 0.1), N V λ1242.804 (6 km s^{-1} away from an Fe II line with optical depth of about 0.2) and O IV λ1404.812 (3.2 km s^{-1} away from an Fe II line with optical depth of ~ 0.2).

Some of the above wavelength coincidences may be of some importance in exciting Fe^+ atoms to high energy levels, but they cannot explain the wealth of strong high energy Fe II transitions observed in quasars. We include in the calculation the two that we find to be most important considering conditions (*i*), (*ii*), and (*iii*) above (see below), but different effects must also be considered.

Another possibility, which was not considered in earlier work, is fluorescence among different Fe II lines. To investigate this process we checked most of the optically thick Fe II lines in our list for wavelength coincidences. We adopted a Gaussian absorption profile and used a criterion of 7.5 km s^{-1} or less between line centers. This assures a large conversion efficiency between optically thick lines since, for large optical depths, most scattering occurs within three Doppler widths of the line core. The coincidences found are listed in Table 1. (Table 1 is thought to include most of the important coincidences, although we do not claim completeness.)

Our list consists of 163 line coincidences and contains, we believe, the transitions most likely to be affected by fluorescence. Many of the lines do not appear in Moore (1945, 1950), and no multiplet names are given. δv denotes velocity difference between line centers in km s^{-1}. We do not list transitions where only one of the components is in our multiplet list (i.e., the other line leads to a level that is not included in our list). Wavelength coincidence is important for many more lines if large turbulent motions are taking place, increasing the probability of line overlapping. The large number of high energy levels that are likely to be populated by line fluorescence demonstrates the potential importance of this process. The final column of Table 1 gives those multiplets observed in RR Tel that arise from the upper energy level (given in parentheses) populated by the fluorescence. We have also checked several strong lines in the spectrum of RR Tel that arise from odd parity levels *not included* in our scheme. For many of them we could find a wavelength coincidence that can explain the pumping of these levels. The process seems to be of greater importance than fluorescence with lines of other elements, in affecting the level populations of Fe^+.

To evaluate the fluorescence efficiency, consider a simple three-level atom, with lower level, 1, and upper levels 2 and 3. The wavelengths λ_{12} and λ_{13} coincide to three Doppler widths so absorption of a photon can excite the atom from level 1 to either 2 or 3. Let a_{12} and a_{13} be the photon absorption probabilities in the two transitions, and α_2 and α_3 the outside contributions to levels 2 and 3 (mainly due to collisions from other

TABLE 1

Fe II FLUORESCENCE LINE PAIRS

Wavelength	Transition	Multiplet	Wavelength	Transition	Multiplet	δv	RR Tel
1588.290	$a^4F - x^4G^o$	UV 44	1588.326	$a^4F - y^2G^o$		6.8	
1613.004	$a^4F - z^2P^o$		1613.025	$a^4F - z^2F^o$		3.9	
1623.707	$a^4F - z^2F^o$		1623.714	$a^6D - z^4I^o$		1.3	
1629.160	$a^6D - y^6P^o$	UV 8	1629.145	$a^6D - y^4F^o$		2.8	
1631.123	$a^6D - y^6P^o$	UV 8	1631.110	$a^4F - z^2F^o$		3.3	
1640.152	$a^4F - y^4G^o$	UV 43	1640.150	$a^4D - y^4F^o$		0.4	
1709.553	$a^4F - y^4F^o$	UV 37	1709.524	$a^4P - w^4F^o$		5.1	
1714.676	$a^4F - y^2D^o$		1714.710	$a^4F - z^4H^o$		6.0	
1724.851	$a^4F - x^4G^o$		1724.853	$a^2F - z^2D^o$	UV 39	0.4	
1760.339	$a^2G - w^4D^o$		1760.377	$a^2G - w^4F^o$	UV100	6.5	
1776.751	$a^2G - w^4D^o$		1776.789	$a^2G - w^4F^o$	UV100	6.4	
1930.915	$b^4P - w^4D^o$		1930.871	$a^2H - x^4H^o$	UV123	6.8	
1933.417	$a^4F - y^4P^o$		1933.430	$a^2D - w^4F^o$		2.0	
1936.794	$a^6D - z^8P^o$	UV 7	1936.805	$a^2G - y^4H^o$	UV 96	1.7	
1975.595	$b^4P - w^4D^o$		1975.548	$a^2G - y^4H^o$		7.1	
1993.912	$b^4P - w^2D^o$		1993.901	$a^2G - x^4F^o$	UV 95	1.7	
1999.730	$a^2D - x^2G$		1999.724	$a^4P - x^4D^o$	UV 83	0.9	
2005.710	$b^4F - w^4D^o$	UV187	2005.759	$b^4F - w^4F^o$	UV186	7.3	
2010.952	$a^2G - z^2H^o$	UV 94	2010.916	$b^4F - w^2D^o$	UV187	5.4	
2019.825	$b^4F - w^4D^o$	UV187	2019.829	$b^4F - x^2H^o$		0.6	
2031.569	$b^4F - w^4F^o$	UV186	2031.580	$a^6S - w^4D^o$		1.6	
2032.613	$a^4F - z^6P^o$		2032.624	$b^4F - w^4P^o$		1.6	
2071.791	$a^2P - x^4F^o$	UV107	2071.806	$a^4P - y^4D^o$		2.2	
2094.977	$a^2G - y^4G^o$	UV 91	2094.996	$a^2P - x^4G^o$		2.7	
2097.548	$a^4P - y^4P^o$	UV 80	2097.508	$a^2H - y^2H^o$	UV120	5.7	
2110.724	$a^4P - y^4F^o$	UV 80	2110.734	$a^2P - z^4S^o$	UV108	1.4	
2133.956	$a^4G - w^2D^o$		2134.011	$a^4G - w^4F^o$	UV213	7.7	
2134.576	$a^4G - x^2H^o$	UV212	2134.624	$b^2P - w^2D^o$	UV226	6.8	
2140.143	$b^4F - y^2F^o$		2140.169	$a^2H - y^2H^o$	UV120	3.6	
2159.160	$a^6D - z^2P^o$	UV 6	2159.190	$b^4H - w^2D^o$		4.2	
2159.666	$a^6S - y^2F^o$		2159.658	$a^4H - y^2H^o$		0.3	
2169.864	$a^2H - y^4H^o$	UV119	2169.878	$b^4F - x^2P^o$	UV185	1.9	
2177.526	$a^4G - w^4P^o$		2177.542	$b^2H - x^2H^o$	UV247	2.2	
2183.522	$a^4H - y^4H^o$	UV119	2183.572	$a^2G - y^4F^o$	UV 89	6.9	
2183.572	$a^2G - y^2F^o$	UV 89	2183.578	$b^4P - x^4F^o$		0.8	
2183.790	$b^2H - x^2H^o$	UV247	2183.836	$a^2F - w^2G^o$		6.3	
2204.057	$a^2G - y^4D^o$		2204.105	$a^2H - x^4G^o$		6.5	
2206.595	$a^2F - w^4D^o$		2206.592	$a^2D - x^4F^o$	UV134	0.4	
2237.808	$a^2P - x^4D^o$		2237.824	$a^4G - z^2G^o$		2.1	
2246.059	$a^4F - z^4P^o$		2246.026	$a^4G - x^2G^o$		4.4	
2248.089	$a^2P - y^4D^o$		2248.097	$a^4G - x^4G^o$		1.1	
2254.406	$a^6D - z^4D^o$	UV 5	2254.394	$a^4D - z^8P^o$		1.6	
2254.383	$a^2F - w^4P^o$		2254.394	$a^2D - z^2P^o$		1.5	
2254.383	$a^2F - w^2P^o$		2254.406	$a^6D - z^4D^o$	UV 5	3.1	
2255.149	$a^2P - y^4D^o$		2255.190	$a^4H - x^4G^o$		5.5	
2258.387	$a^4H - x^4G$		2258.360	$b^4P - x^2G$		3.6	
2262.226	$a^4F - z^8P^o$		2262.247	$b^4F - y^2D^o$		2.8	
2268.823	$a^6D - z^4D^o$	UV 5	2268.871	$b^4F - y^2D^o$		6.4	
2276.814	$a^4F - z^4P^o$		2276.763	$a^2D - z^2F^o$	UV132	6.7	
2279.175	$b^4F - y^4H^o$		2279.128	$b^2P - y^4F^o$		6.2	
2283.485	$a^6D - z^4D^o$	UV 5	2283.514	$b^4F - y^4H^o$		3.8	UV168,UV209,UV282 (y^4H^o)
2284.240	$a^4F - z^6F^o$	UV 33	2284.236	$b^4F - x^4D^o$	UV179	0.5	
2293.131	$a^4G - y^2F^o$		2293.143	$b^4P - z^2F^o$		1.6	
2309.024	$a^6S - x^4F^o$		2309.072	$b^4F - x^4G^o$	UV183	6.2	
2318.345	$b^4F - x^4G^o$	UV183	2318.357	$a^4G - x^4P^o$		1.6	
2318.345	$b^4F - x^4G^o$	UV183	2318.396	$a^4H - y^2G^o$	UV167	6.6	
2318.357	$a^4G - x^4P^o$		2318.396	$a^4H - y^4G^o$	UV167	5.1	
2321.647	$a^6S - x^4F^o$		2321.691	$b^4F - x^4G^o$	UV167	5.7	
2322.331	$b^4F - x^4G^o$	UV183	2322.331	$a^4G - x^4P^o$		0.0	
2345.945	$a^6S - x^4G^o$		2345.964	$b^4P - z^2F^o$		2.4	
2348.115	$a^4F - z^2D^o$	UV 36	2348.109	$a^6H - z^6F^o$	UV166	0.8	UV181 (z^2F^o)
2348.243	$a^4G - y^2H^o$	UV211	2348.303	$a^6D - z^6P^o$	UV 3	7.7	
2355.215	$a^4P - y^4P^o$		2355.256	$a^2D - y^4D^o$	UV130	5.2	
2355.216	$a^4H - y^4G^o$	UV165	2355.215	$a^2P - y^4P^o$		0.1	
2355.216	$a^4H - y^4G^o$	UV165	2355.256	$a^2D - y^2D^o$	UV130	5.1	
2359.133	$a^4H - y^4G^o$	UV165	2359.106	$a^6D - z^6P^o$	UV 3	3.4	

TABLE 1—*Continued*

Wavelength	Transition	Multiplet	Wavelength	Transition	Multiplet	δv	RR Tel
2366.876	$a^4H - y^4G^o$	UV165	2366.857	$a^6D - z^6F^o$	UV 2	1.1	
2369.240	$b^4F - y^4G^o$	UV182	2369.200	$a^4G - y^4H^o$	UV211	5.1	
2370.499	$a^6F - z^6F^o$	UV 35	2370.466	$a^4D - y^4D^o$	UV130	4.2	UV148,UV218 (y^4D^o)
2373.736	$a^6D - z^6F^o$	UV 2	2373.757	$b^4P - x^4D^o$		2.7	
2391.478	$a^4F - z^4F^o$	UV 35	2391.457	$b^4F - z^4P^o$		2.6	
2394.893	$a^4H - z^4G^o$	UV116	2394.948	$b^4G - x^4H^o$	UV286	6.9	
2399.233	$a^4F - z^4D^o$	UV 36	2399.242	$a^6D - z^6F^o$	UV 2	1.1	
2399.961	$a^2D - y^6P^o$		2399.990	$a^2D - y^4D^o$	UV130	3.6	
2402.599	$a^4F - z^4D^o$	UV 36	2402.616	$a^4D - z^4D^o$	UV129	2.1	
2402.599	$a^4F - z^4D^o$	UV 36	2402.629	$b^4D - w^4G^o$	UV303	3.8	
2402.616	$a^2D - z^2D^o$	UV129	2402.629	$b^4D - w^2G^o$	UV303	1.6	
2407.939	$a^2H - z^2G^o$	UV116	2407.952	$a^6S - z^4P^o$		1.6	
2421.901	$a^4H - z^4G^o$	UV116	2421.918	$b^4F - y^4G^o$	UV180	2.1	
2424.651	$b^4F - y^4G^o$	UV180	2424.591	$b^4D - w^4D^o$	UV301	7.4	
2425.362	$b^4P - y^6P^o$		2425.364	$a^4G - y^4D^o$	UV210	0.3	
2429.388	$b^4P - y^4D^o$	UV148	2429.418	$b^4P - x^4D^o$		3.7	
2434.952	$b^4F - y^4G^o$	UV180	2435.003	$b^4P - x^4D^o$		6.3	
2447.627	$a^2D - y^4F^o$	UV131	2447.567	$b^4D - w^4P^o$	UV299	7.4	
2449.729	$a^4F - z^6P^o$	UV 34	2449.778	$b^4F - w^4D^o$	UV312	6.0	
2451.219	$a^4G - y^4H^o$	UV209	2451.259	$a^4F - z^6P^o$	UV 34	4.9	UV168,UV209,UV282 (y^4H^o)
2459.114	$a^2H - z^2G^o$	UV163	2459.109	$b^2F - w^4D^o$	UV312	0.6	
2463.738	$a^2D - z^2D^o$	UV129	2463.720	$b^4D - w^4P^o$	UV299	2.2	
2463.737	$a^4H - y^2F^o$	UV162	2463.720	$b^4D - w^4P^o$	UV299	2.1	
2463.738	$a^2D - z^2D^o$	UV129	2463.737	$a^4H - y^2F^o$	UV162	0.1	
2468.257	$b^4P - y^4P^o$	UV145	2468.300	$a^2H - z^2G^o$	UV163	5.2	
2472.074	$a^4H - y^4F^o$	UV162	2472.063	$a^2D - z^4G^o$		1.3	
2473.323	$b^4P - y^4D^o$	UV148	2473.347	$b^2H - y^4H^o$	UV243	2.9	
2477.345	$a^4H - y^4F^o$	UV162	2477.384	$b^2F - w^4F^o$	UV311	4.7	
2484.201	$a^4F - z^6F^o$	UV 33	2484.236	$b^4H - y^4H^o$	UV243	2.2	UV168,UV209,UV282 (y^4H^o)
2484.201	$a^4F - z^6F^o$	UV 33	2484.236	$b^2F - x^4D^o$	UV279	2.2	
2484.247	$b^2H - y^4H^o$	UV243	2484.236	$b^4H - y^4H^o$	UV243	1.3	
2484.247	$b^2H - y^4H^o$	UV243	2484.236	$b^4F - x^4D^o$	UV279	1.3	
2484.247	$b^2H - y^4H^o$	UV243	2484.201	$a^4F - z^6F^o$	UV033	5.6	UV168,UV209,UV282 (y^4H^o)
2484.236	$b^2H - y^4H^o$	UV243	2484.236	$b^4F - x^4D^o$	UV179	0.0	
2484.572	$b^2H - y^4H^o$	UV243	2484.527	$b^4P - y^6P^o$		5.4	
2489.846	$a^2H - z^4G^o$	UV112	2489.831	$a^4G - x^4G^o$	UV207	1.8	
2491.386	$b^4P - z^4G^o$	UV146	2491.398	$a^4G - x^4G^o$	UV207	1.4	
2493.184	$a^4H - z^4I^o$	UV161	2493.223	$a^4G - x^4G^o$	UV207	4.7	
2493.262	$a^4H - z^4I^o$	UV161	2493.223	$a^4G - x^4G^o$	UV207	4.7	UV198,UV231 (z^4I^o)
2493.295	$a^4F - z^6F^o$	UV 33	2493.262	$a^4H - z^4I^o$	UV161	4.0	
2494.144	$a^4H - z^4H^o$	UV113	2494.116	$a^4H - z^4I^o$	UV161	3.4	
2497.683	$b^4F - z^2I^o$		2497.716	$b^2H - x^4F^o$	UV242	3.6	
2497.703	$a^2D - y^4P^o$	UV128	2497.683	$b^4F - z^2I^o$		2.4	
2497.703	$a^2D - y^4P^o$	UV128	2497.716	$b^2H - x^4F^o$	UV242	1.6	
2497.820	$b^4F - y^4D^o$	UV175	2497.820	$a^4G - x^4G^o$	UV207	0.0	
2510.528	$a^4F - z^6P^o$	UV 34	2510.565	$a^2H - z^4G^o$	UV112	4.4	UV158,UV195,UV216 (z^4G^o)
2514.933	$b^4F - y^4D^o$	UV175	2514.906	$a^4G - z^2H^o$	UV206	3.2	
2519.103	$a^4F - z^6F^o$	UV 33	2519.048	$a^2F - y^2D^o$	UV268	6.6	
2519.071	$b^4F - z^2G^o$	UV178	2519.048	$a^2F - y^2D^o$	UV268	2.7	UV258,OP 66 (z^2G^o)
2519.103	$a^4F - z^6F^o$	UV 33	2519.071	$b^4F - z^2G^o$	UV178	3.8	
2526.076	$a^4H - z^4H^o$	UV159	2526.110	$a^4G - z^2H^o$	UV206	4.0	
2527.104	$a^4H - z^4H^o$	UV159	2527.157	$a^4G - z^2H^o$	UV206	6.3	
2529.559	$b^4P - y^4P^o$	UV145	2529.546	$b^4F - y^4F^o$	UV177	1.5	
2534.419	$a^4H - z^4H^o$	UV159	2534.356	$b^4F - z^2G^o$	UV178	7.5	
2536.806	$a^4H - z^4H^o$	UV159	2536.845	$a^4H - z^4H^o$	UV159	4.6	
2538.204	$b^2H - z^2H^o$	UV240	2538.205	$a^2I - x^2H^o$	UV319	0.1	
2543.431	$b^4F - y^4F^o$	UV177	2543.380	$a^4H - z^4H^o$	UV159	6.0	
2543.431	$b^4F - y^4F^o$	UV177	2543.484	$a^4G - y^2G^o$	UV205	6.3	
2551.204	$c^2G - w^4D^o$	UV238	2551.151	$b^4F - z^2D^o$	UV173	6.2	
2557.151	$a^2D - y^4P^o$	UV128	2557.151	$b^4F - z^2D^o$	UV173	0.0	
2557.084	$a^4H - z^4G^o$	UV158	2557.151	$a^2D - y^4P^o$	UV128	7.9	
2573.211	$a^4G - y^2G^o$	UV205	2573.181	$c^2G - w^4F^o$	UV327	3.5	
2577.923	$a^4F - z^4P^o$	UV 64	2577.967	$a^4G - z^2P^o$		5.1	
2579.413	$b^2H - y^2G^o$		2579.415	$a^2F - x^4F^o$	UV266	0.2	
2588.193	$b^4P - y^4P^o$	UV145	2588.142	$a^4P - z^8P^o$		5.9	
2595.303	$b^4F - z^4H^o$	UV172	2595.278	$a^4G - y^4G^o$	UV203	2.9	

TABLE 1—*Continued*

Wavelength	Transition	Multiplet	Wavelength	Transition	Multiplet	δv	RR Tel
2607.089	$a^6D - z^6D^o$	UV 1	2607.023	$b^4F - z^4H^o$	UV172	7.6	
2611.074	$a^4F - z^4P^o$	UV 64	2611.138	$b^4D - y^2F^o$	UV297	7.4	
2614.903	$a^4G - z^2F^o$	UV204	2614.871	$b^4F - z^4G^o$	UV171	3.7	
2626.501	$b^4F - z^2D^o$	UV173	2626.472	$b^4D - x^4P^o$	UV296	3.3	
2626.698	$a^4G - y^4G^o$	UV203	2626.748	$b^4D - x^4P^o$	UV296	5.7	
2631.048	$a^6D - z^6D^o$	UV 1	2631.011	$b^4F - z^2G^o$	UV171	4.2	UV158,UV195,UV216 (z^4g^o)
2635.397	$b^4D - x^4P^o$	UV296	2635.401	$b^2H - z^2F^o$	UV238	0.5	
2645.082	$a^4F - y^2G^o$	UV263	2645.084	$b^2F - y^2F^o$	UV309	0.2	
2692.834	$a^2F - z^4F^o$	UV 62	2692.857	$a^2F - z^2F^o$	UV261	2.6	UV181 (z^2F^o)
2728.907	$a^2F - y^4G^o$	UV260	2728.863	$a^4G - y^4D^o$		4.8	
2739.548	$a^4F - z^4D^o$	UV 63	2739.511	$b^2H - z^2I^o$	UV235	4.1	UV235 (z^2I^o)
2746.484	$a^4F - z^4F^o$	UV 62	2746.519	$b^2D - w^4D^o$		3.8	
2749.181	$a^4F - z^4D^o$	UV 63	2749.162	$b^2P - y^4F^o$		2.1	
2755.737	$a^4F - z^4F^o$	UV 62	2755.694	$a^4G - z^2G^o$	UV200	4.7	UV258,OP 66 (z^2G^o)
2762.447	$a^4G - y^4F^o$	UV199	2762.379	$a^4G - y^6P^o$		7.4	
2770.502	$a^4G - y^4F^o$	UV199	2770.505	$a^4G - z^4I^o$	UV198	0.3	
2777.890	$b^2H - y^4F^o$	UV233	2777.827	$b^2G - x^4F^o$	UV281	6.8	
2783.404	$b^2D - w^4P^o$		2783.447	$b^2D - w^4F^o$	UV338	4.6	
2785.024	$a^4F - z^6D^o$	UV032	2784.979	$b^2P - y^4D^o$	UV218	4.9	UV148,UV218 (y^4D^o)
2857.420	$a^4G - z^4G^o$	UV195	2857.475	$a^2S - w^4P^o$		5.8	
2858.333	$a^4G - z^2G^o$	UV195	2858.341	$b^2G - z^2H^o$	UV279	0.8	
2871.060	$a^4G - z^4G^o$	UV195	2871.131	$b^2H - z^4H^o$	UV230	7.4	
2886.266	$b^2H - z^4H^o$	UV230	2886.236	$b^2H - z^4G^o$	UV229	3.1	
2917.466	$a^4F - z^6P^o$	UV 61	2917.453	$b^2F - x^2G^o$	UV307	1.3	
2964.623	$a^4P - z^4P^o$	UV 78	2964.659	$a^2D - z^6F^o$	UV 60	3.6	
2984.825	$a^4P - z^4P^o$	UV 78	2984.889	$a^2F - z^4G^o$	OP 60	6.4	UV158,UV195,UV216 (z^4G^o)
3183.114	$a^4P - z^4F^o$	OP 7	3183.070	$b^2G - y^6P^o$		4.2	
3193.799	$a^4P - z^4D^o$	OP 2	3193.768	$b^2D - y^4D^o$	OP 79	2.9	UV148,UV218 (y^4D^o)
3193.799	$a^2P - z^4D^o$	OP 6	3193.859	$b^2G - y^2F^o$	OP 67	5.6	
3251.290	$b^2G - z^4I^o$		3251.349	$b^2D - y^2D^o$	OP137	5.4	
3532.681	$b^2D - z^2F^o$	OP132	3532.682	$b^4D - z^4S^o$	OP 74	0.1	

levels), then:

$$\alpha_2 + N_3 A_{31} a_{12} = N_2 A_{21}(1 - a_{12}) \qquad (10)$$

and

$$\alpha_3 + N_2 A_{21} a_{13} = N_3 A_{31}(1 - a_{13}). \qquad (11)$$

The local escape probability is the same for the two transitions and is given by:

$$\varepsilon_{12} = \varepsilon_{13} = 1 - a_{12} - a_{13}, \qquad (12)$$

and the line emissivity is:

$$I(\lambda_{12}) = h\nu_{12}\varepsilon_{12}(N_2 A_{21} + N_3 A_{31}). \qquad (13)$$

These equations can be used to solve for the upper level populations N_2 and N_3. We include a simple generalization of this scheme in our calculations of the level populations using, in turn, all the line pairs of Table 1. We do this in each layer, considering the inward and outward directions separately. In our scheme $\varepsilon = \varepsilon(\tau_{12} + \tau_{13})$ where ε is given by equation (3) and a_{12}/a_{13} is estimated mainly from the local level populations. This approach is appropriate since most line scattering occurs within the Doppler core, without much diffusion in space.

A main source of uncertainty in calculating line fluorescence is our treatment of the whole multiplet, rather than individual transitions. Collisional mixing of odd-parity levels will distribute the fluorescence contribution among other levels in the term, provided collisions are fast enough. This of course depends on the electron density in the cloud and is not always a good approximation (see § II*c* above). In an attempt to correct for this, we introduce an efficiency factor, which can vary from 0 (no fluorescence) to 1 (100% fluorescence efficiency). Only that fraction of line photons is assumed to be affected by fluorescence. This factor depends on the turbulent velocity, V_t, and the number of lines in the multiplet (i.e., it is smaller if only one out of 10 lines in a multiplet coincides in wavelength with another line, compared, with a case of one out of three or four lines). In principle the efficiency is different for each multiplet pair, but in practice it is not possible to assess its value accurately. Therefore we choose it to be between 0.1 and 0.3 for all transitions, for cases of $V_t \approx 5$ km s^{-1}. For larger V_t it can be larger, perhaps

0.3–0.5. A point to note here is that increasing fluorescence gives weaker optical lines. The reason is that most optical transitions arise from low lying levels, and the population of these is reduced when the fluorescence efficiency is increased. The criterion of ≤ 7.5 km s^{-1} separation between line centers is adequate for all cases from pure thermal motion at $T_e \geq 7500$ K (Doppler width of ~ 1.5 km s^{-1}) to $V_t \simeq 10$ km s^{-1}. The nature of the problem changes significantly at larger velocities, where many more lines overlap. We do not investigate the general properties of such cases here since complicated dynamical considerations are involved. Instead we extend our simple approximation to all cases, even those having $V_t > 10$ km s^{-1}.

Finally we comment on the most important wavelength coincidences with other elements described earlier. Fe II λ2801.599 is 11.35 km s^{-1}, or about seven Doppler widths, from the center of Mg II λ2802.704. When included in the calculations we find that up to one-third of the Mg II line photons (i.e., one-ninth of the Mg II λ2798 doublet intensity) is absorbed. This has little effect on the shape and intensity of the Fe II bands. In most cases the optical depth in Fe II λ2802.599 is small, and the effect negligible. C IV λ1548.185 is close to Fe II λ1548.204 (3.7 km s^{-1}). The Fe II line optical depth is large (> 5), but the two lines do not form in the same region of the cloud. We include it by adding half the C IV λ1548.2 photons to the incident continuum flux. It is hard to estimate the fractional destruction of C IV λ1548.2 photons due to this. The two lines have very different thermal widths, and C IV λ1548.2 emission profile is doubled (i.e., nearly zero intensity close to the line center) in the Fe II zone. We find neither a significant enhancement of Fe II transitions nor a significant destruction of C IV λ1548.2 due to this coincidence. We do not include other lines although fluorescence with Lyβ may contribute to the feature observed at ~ 2070 Å. At most, such fluorescence will be as strong as O I λ1302, which is also excited by Lyβ. The optical depth in the Fe II line in question is, however, very small and the maximum intensity will probably not be reached.

f) *Charge Exchange*

Johansson (1978*b*) noted that charge transfer reactions can lead to overpopulation of some high energy levels of Fe^+. This may be related to the observed Fe II lines in some stars. We do not consider this process to be important in active nuclei since neither the Fe^0 nor the Fe^{++} abundance in our model is large enough to explain the observed strength of the high energy Fe II transitions.

III. RESULTS AND DISCUSSION

In this section we give several examples of our new calculations and discuss the dependence of the Fe II spectrum on the model parameters. We defer the detailed comparison with observations to the second paper, where we consider the relationship between Fe II emission and spectral features such as Balmer lines and continuum.

a) *RR Telescopii*

RR Tel is a well-known, extensively studied symbiotic star (Penston *et al.* 1983, and references therein). It exhibits an extremely rich Fe II spectrum in which several hundred lines have been identified. The detailed observations by Thackeray (1977) and Penston *et al.* (1983) are most useful for testing the suggestion of line fluorescence and its influence on the excitation of high energy levels.

Penston *et al.* (1983) list many Fe II ultraviolet lines calibrated on an absolute flux scale, with wavelengths accurate to ~ 0.3 Å. Thackeray's (1977) spectrograms were not absolutely calibrated, but he estimated relative line intensities and the wavelengths for unblended lines are accurate to ~ 0.1 Å. We have put these two lists on the same flux scale by adjusting the intensity of several weak optical and ultraviolet He II lines, to fit their predicted case B intensities. He II 4686 could not be used, since it was probably saturated in Thackeray's (1977) observations. This can be seen by comparing its listed strength with those of He II λ5412 and He II λ4541.[1] Figure 2 (*top*) shows the full 1500–6000 Å Fe II spectrum obtained by combining the two sources.

The physical conditions in the line emitting region of RR Tel have been discussed, briefly, by Penston *et al.* (1983). Here we restrict our attention to the Fe II spectrum. We assume a simple, uniform Fe II zone, with $N_e = 10^6$ cm^{-3} and $T_e = 10^4$ K throughout. This zone is at the back of the more highly ionized H^+ zone. We take $\tau(2324) = 3 \times 10^4$, $V_t = 5$ km s^{-1} and assume no absorption of continuum photons. Results of the calculations are shown in Figure 2 (*bottom*). Comparison with the observed spectrum in Figure 2 (*top*) shows good overall agreement. Several of the high energy transitions that could not be explained in other ways are naturally produced by line fluorescence. Several other lines arising from transitions not included in our list can also be explained by line fluorescence with known transitions. We cannot explain Fe II lines with even-parity upper levels. Perhaps collisions from high energy odd-parity levels are important. Note here that there are lines in the models that do not show in the observations, because line fluorescence may excite only one or two lines in a multiplet, while our model includes all such lines. Figure 2 (*bottom*) demonstrates the large number of lines included in the calculations, and the usefulness of such

[1]Even though the emission-line spectrum of RR Tel is variable with time, Surdej (Penston *et al.* 1983) finds "no striking changes" between Thackeray's spectra and two others obtained near the time of the observations of the ultraviolet spectra.

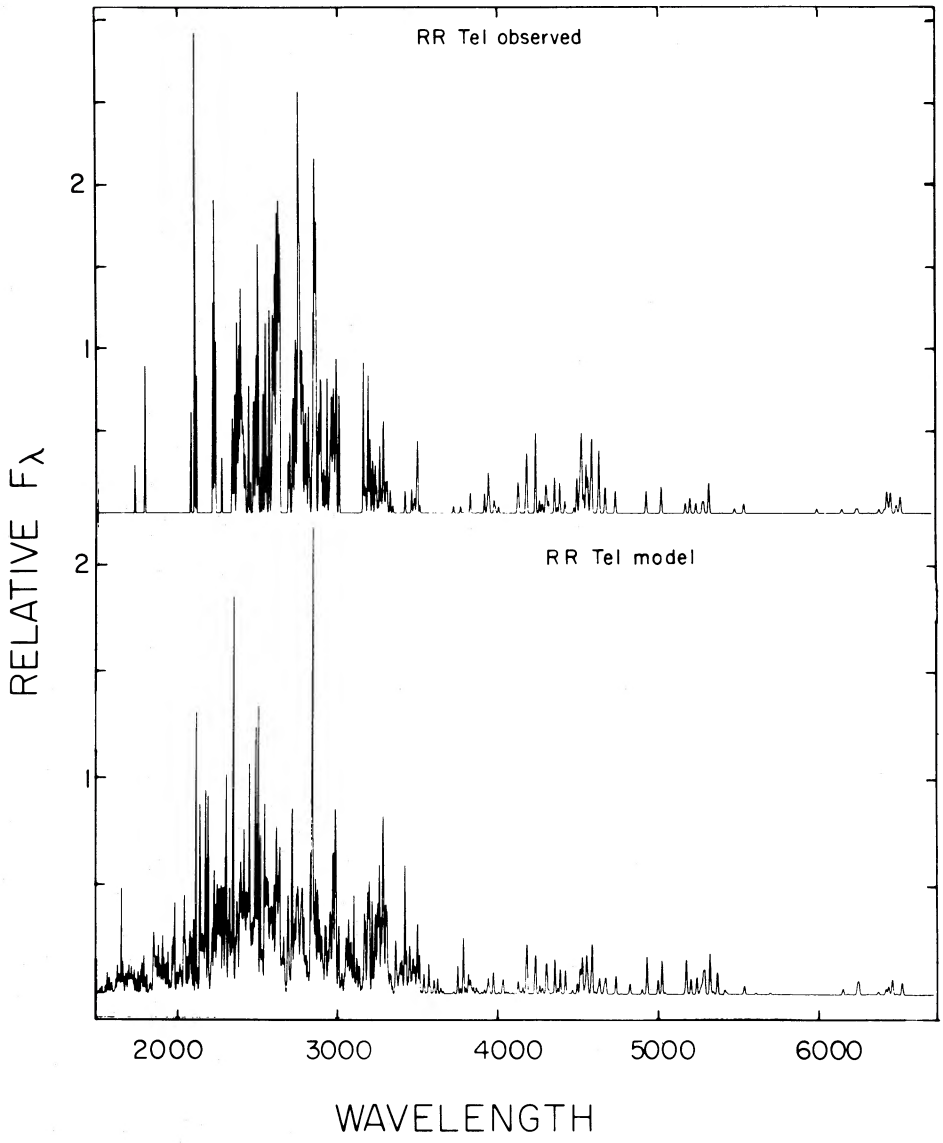

FIG. 2.—The Fe II spectrum of RR Tel. (*top*) Observed (Thackeray 1977; Penston *et al.* 1983); (*bottom*) calculated (see text).

models in the understanding of a variety of astronomical objects.

We have also looked at the spectra of some late-type stars (van der Hucht *et al.* 1978), Eta Carinae (Johansson 1977), and V1016 Cyg (Nussbaumer and Schild 1981) to verify that many of the high energy Fe II transitions there can be explained via line fluorescence. We believe that a model for these objects, like the one presented here for RR Tel, can be as successful in fitting their Fe II spectra. We also found indications of this process in several (unpublished) spectra of other novae and symbiotic stars. We do not present models for these objects here since our aim is to explain quasar spectra.

b) Quasars and Seyfert Galaxies

To demonstrate some of the more important features of our model, we choose one case, shown in Figure 1, and vary in it the values of V_t, $\tau(2343)$, and the fluorescence efficiency [note again that $V_t \times \tau(2343) = const$ for a given photoionization model]. In the following examples we assume that the observed profiles of all lines are Gaussian with $1/e$ half-width of 3000 km s^{-1} (not to be confused with the turbulent velocity inside one cloud, V_t).

Figure 3 shows calculations and results for $V_t = 8$ km s^{-1} and no line fluorescence. Comparisons with

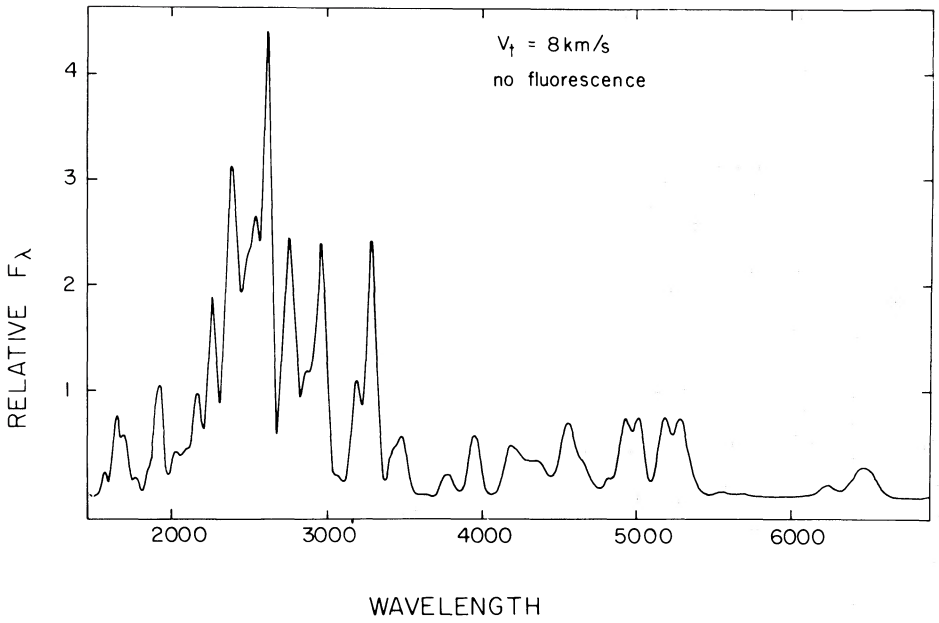

FIG. 3.—Standard quasar Fe II spectrum for a case of no line fluorescence. This spectrum is quite similar in its relative multiplet strengths to those calculated theoretically by Netzer (1980), Kwan and Krolik (1981), Joly (1981), and Grandi (1981). It is very different from most observed spectra, where many of the "gaps" are filled by high energy Fe II transitions.

observations, like those in Papers II and III, demonstrate some of the difficulties encountered in previous Fe II models. The agreement in shape and strength of most features is poor, and there are many gaps in the spectrum, such as around 2440 Å, that can only be filled by high energy transitions. This is typical of all previous Fe II calculations known to us, including Paper I (Table 2 there), Kwan and Krolik (1981, Table 5 there) and Joly (1981). All these authors have succeeded in producing the *total* Fe II line intensity but have failed to produce the observed shape.

Recently Grandi (1981), using Phillips's unpublished calculations, realized the above difficulty and discussed, in much detail, the bad agreement in some wavelength regions. He suggested that numerous high excitation Fe II lines are present and arbitrarily adjusted the multiplet strengths to give agreement with the observations. We agree with Grandi's (1981) suggestion that high excitation Fe II lines are indeed very strong. Furthermore, we propose that Fe II line fluorescence is the process responsible for populating the Fe^+ high energy levels. This is evident from inspection of Figure 4, where three cases of the standard model, with line fluorescence included, are shown. In these cases V_t ranges from 3 to 20 km s^{-1} and $\tau(2343)$ changes accordingly. All the previous gaps are now filled, and the theoretical spectrum resembles many observed ones. There is also strong Fe II emission at $\lambda \sim 2100$ Å, $\lambda \sim 1900$ Å, and $\lambda \sim 1650$ Å, as required by the observations (Paper III). All the strong multiplets with intensity ≥ 0.03 the intensity of UV1 are marked on the diagram where space permits. Many of these do indeed come from high energy levels, including some that are not included in the Moore (1945, 1950) multiplet tables.

The relative strengths of the optical Fe II lines increase with decreasing V_t for three reasons: (*i*) large optical depth results in more scattering of the resonance line photons; (*ii*) large Fe II optical depth is associated with larger Balmer opacity, and more destruction of the optically thick, $\lambda < 3646$ Å Fe II lines; and (*iii*) large V_t increases the fluorescence efficiency, which competes with the conversion of resonance line photons into optical ones. Mechanism (*i*) above is not very important, since the relative strength of the optical and ultraviolet Fe II lines does not change much with optical depth, over the range considered here (see also Paper I). Mechanism (*iii*) is also only marginally important, since the fluorescence efficiency in our model does not change by a large factor. Mechanism (*ii*) is more important than the other two, at least in the cases considered here. Destruction of optically thick, $\lambda < 3646$ Å line photons is significant if the scattering takes place in the region where the Balmer continuum opacity is the greatest. This is the case for Mg II λ2798 and Fe II lines, and the mechanism was suggested in Paper I as an important factor in determining these line strengths. Later, Kwan and Krolik (1981) included it in their calculations and reached similar conclusions.

The Balmer continuum opacity is related to $\tau(H\alpha)$ which, in turn, is proportional to $\tau(2343)$ (see Fig. 1).

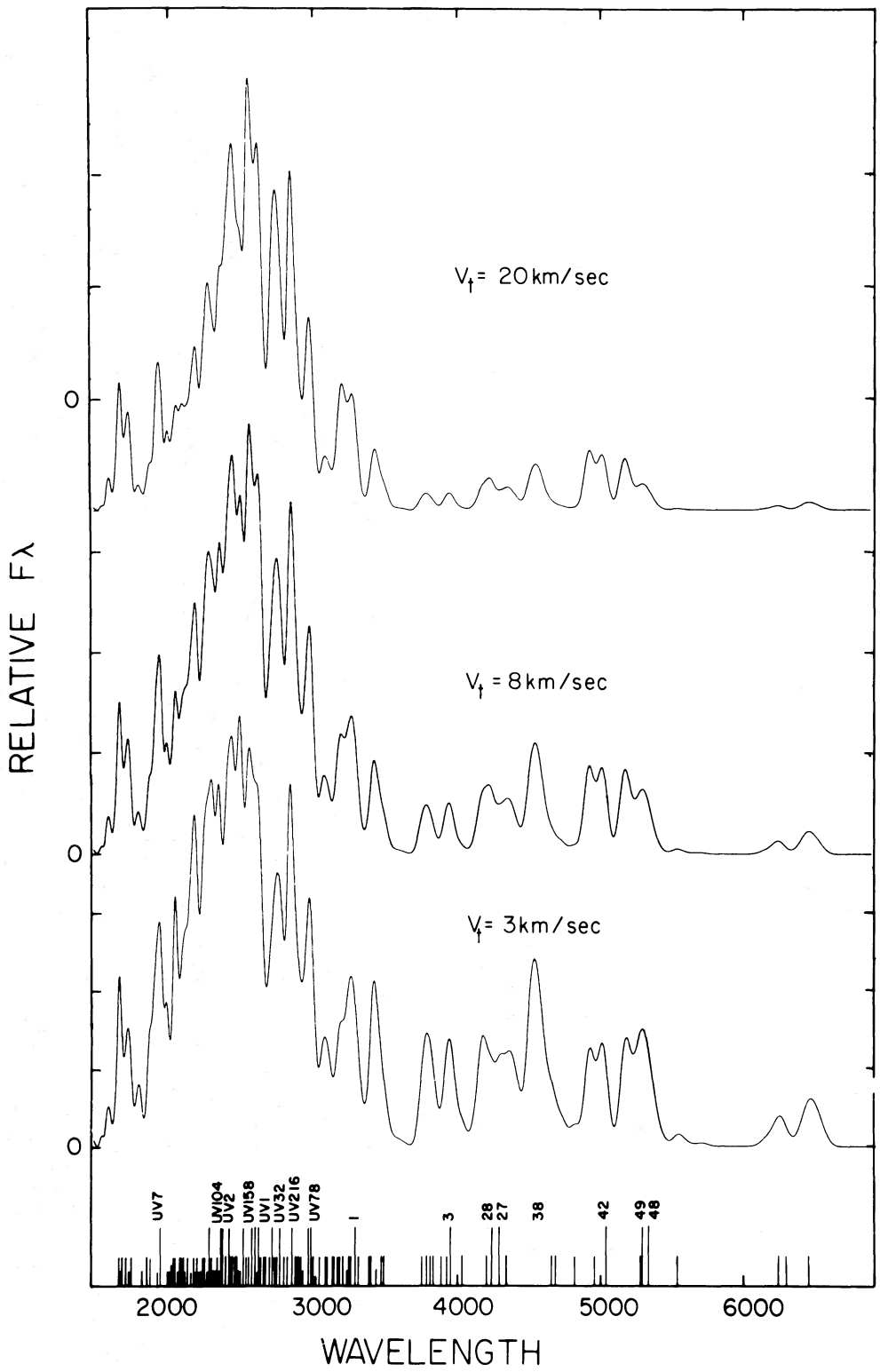

FIG. 4.—Fe II spectra in the standard model with line fluorescence included. The variable parameter is V_t [$V_t \times \tau(2343)$ is the same for all cases]. Note the improved agreement with observed spectra due to the appearance of many high energy transitions. The position of Fe II multiplets with intensities of 3% or more the intensity of UV1 are shown as space permitted. Longest lines marked are those with 30% or more of the intensity of UV1. Shortest ones do not appear in the Moore (1945, 1950) multiplet tables.

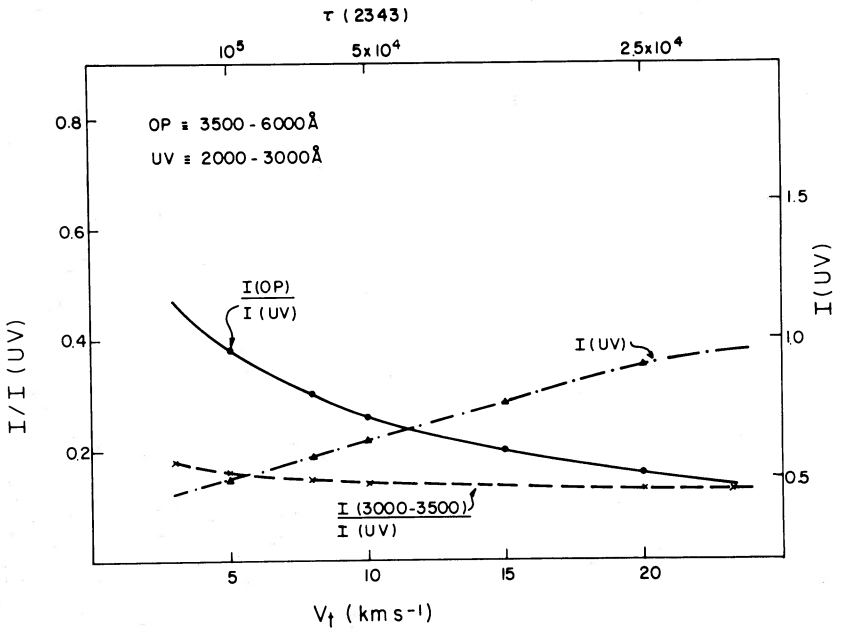

FIG. 5.—Relative strengths of Fe II multiplets in three spectral regions, as a function of $\tau(2343)$ and V_t in the standard model. I(UV) is in units of 10^7 ergs s^{-1} cm^{-2}.

For the set of models considered here

$$\tau(\text{Balmer continuum } 3646\text{ Å}) \simeq 2\times \frac{10\text{ km s}^{-1}}{\left(V_H^2+V_t^2\right)^{1/2}}, \quad (14)$$

where V_H is the hydrogen thermal velocity (of the order of 10 km s^{-1}). Destruction of $\lambda < 3646$ Å resonance lines, by the Balmer continuum, must therefore be important. To evaluate this we use Ferland and Netzer's (1979) calculation of the destruction of line photons by any continuous opacity source (they actually used these results to work out the destruction of multiply scattered line photons in a gas containing dust particles). The calculations give the fractional destruction of photons as a function of the continuum opacity optical depth and the number of scatterings. In the present case the fractional destruction of Fe II lines depends both on the multiplet wavelength (due to the drop in Balmer continuum opacity) and optical depth, as found from the model calculations. For example, in the standard case, we find that ~ 49% of all Fe II photons are destroyed if $V_t = 20$ km s^{-1} and ~ 64% if $V_t = 5$ km s^{-1}. This explains the increase in the relative strength of the optical Fe II lines (which are not affected by the Balmer destruction), with increasing $\tau(2343)$.

We have also calculated the strength of the Mg II λ2798 line assuming the Mg^+ and Fe^+ abundances are the same, across the cloud. This tends to overestimate the relative strength of Mg II λ2798, since for similar abundances of iron and magnesium Fe^+ is more abundant than Mg^+ in most parts (Paper I, Fig. 2). For all models discussed above the summed intensity of *all* Fe II lines is about twice that of Mg II λ2798. Mg II λ2798 is more sensitive to destruction by the Balmer continuum, but its dependence on V_t is rather similar to that of the ultraviolet Fe II lines. We expect that the above intensity ratio can exceed 2 in cases of larger optical depth, more realistic ionization structure for Mg^+, larger ionization parameter or peculiar abundances.

An interesting property of the models shown here, and others, is the change in the relative strength of the optical (λ ≥ 3500 Å), near-UV (3000–3500 Å), and UV (2000–3000 Å) lines. Figure 5 shows this for the standard model, as a function of $\tau(2343)$ and V_t. As the optical depth increases (decreasing V_t), the ultraviolet line intensities get weaker (more destruction and conversion), the relative intensity of the optical lines increases, and the relative strength of the 3000–3500 Å multiplets remains nearly unaffected. The relative strength of the optical and 3000–3500 Å Fe II lines gives, therefore, an indication of conditions within the cloud, such as the total optical depth. This is important when only ground-based spectra are available, for objects like broad line radio galaxies. Our model predicts that many weak optical Fe II objects have strong Fe II emission in the ultraviolet and that differences between objects are due mainly to different optical depth.

To complete the discussion we show, in Figure 6, a case of nearly pure continuum absorption, where colli-

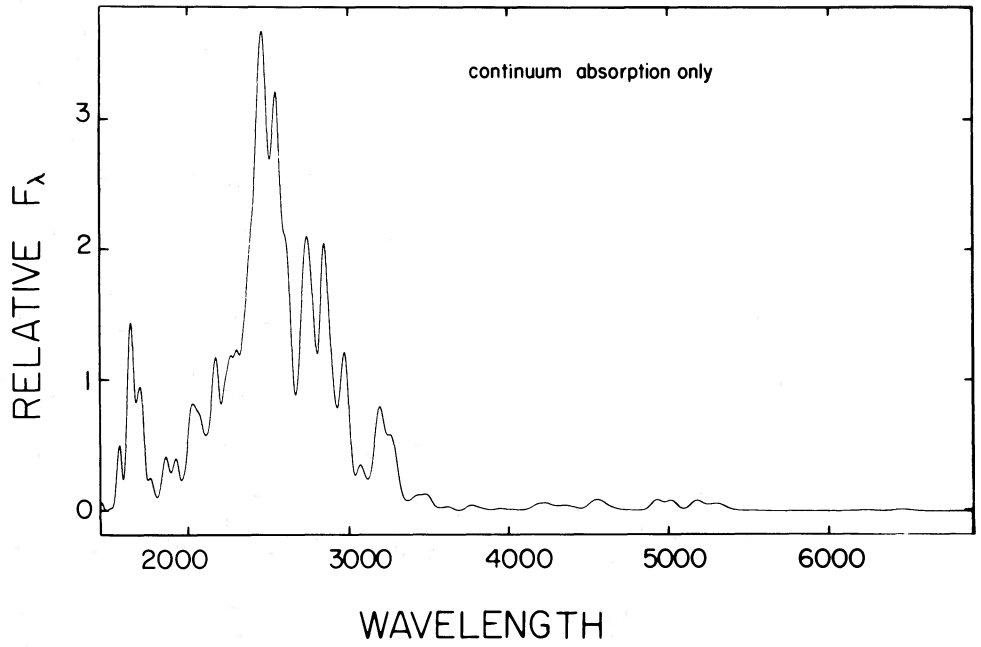

FIG. 6.—Fe II spectrum in a pure continuum absorption model (collisional excitation contributes less than 5% to the lines). Note the extremely weak optical multiplets.

sional excitation is negligible. It was calculated by artificially increasing the number of continuum photons absorbed, but other parameters are as in the standard model with $V_t = 20$ km s^{-1}. The model is characterized by strong ultraviolet lines and extremely weak optical ones. The reason for this, apart from the three effects mentioned above, is the optical depth structure inside the cloud. Most continuum photons get absorbed at the $\tau \sim 1$ point, very close to the inner illuminated face. The inward escape probability, from that location, is very large, and only a few photons are scattered enough times to produce optical transitions. Only in collisional cases, where line photons are created at large optical depths, can the optical line intensity become significant. This argument is an additional point in favor of most excitation being collisional, at least where strong optical Fe II lines are observed.

Finally, we should comment on several emission lines, in the spectrum of quasars, that have been identified in the past as [Fe II] or Fe I lines. Fluorescence excitation of high Fe^+ energy levels results in some of the previously neglected transitions being quite strong. For example, optical multiplets 122, 83, 68, and 123 of Fe II all contribute to a feature near 3070 Å, which was observed by Bergeron and Kunth (1981) and suggested to be an Fe I transition. Optical multiplets 130 and 29 are among the strongest Fe II features in our model and can explain an assumed Fe I line of 3763 Å. The assumed [Fe II] feature at 5158 Å (Oke and Lauer 1979) can be either optical multiplet 35 or 177 of Fe II, and the one near 4244 Å can be one or all of optical multiplets 27, 28, and 151 of Fe II. Some of the [Fe II]–Fe II misidentifications have already been addressed by Joly (1981), but her calculations did not include fluorescence and many high energy level transitions considered by us.

IV. CONCLUSIONS

We have presented a general method for calculating the Fe II line intensities in a model designed to represent quasar photoionized clouds. We have included hundreds of new lines and shown that their large number has some important implications on the emergent spectrum. In particular we have shown that:

(*a*) Radiative excitation of Fe II, through continuum absorption, is important and can contribute up to ~ 20% of the observed flux in ultraviolet Fe II lines.

(*b*) Wavelength coincidences and the overlapping of different Fe II lines are most important and can naturally explain the excitation of many observed high energy transitions in quasars, emission-line stars, and late-type stars. Many unexplained "gaps" typical of previous quasar models, are filled in by the high energy Fe II transitions, and the overall distribution is much smoother.

(*c*) Optical line strengths increase, and ultraviolet line strengths decrease as the optical depth in Fe II is increased. We proposed this as the explanation for the different optical Fe II spectrum seen in different broad line objects. Strong Fe II blends between 3000 and 3500

Å have constant strength relative to the ultraviolet lines and provide an important clue to the nature of weak optical Fe II objects, such as broad line radio galaxies.

This work is supported by The United States-Israel Binational Science Foundation, grant 2305/80, and United States NSF grant AST 79 01182.

REFERENCES

Bergeron, J., and Kunth, D. 1981, *Astr. Ap.*, **85**, L11.
Brown, A., Jordan, C., and Wilson, R. 1979, in *The First Year of IUE*, ed. A. J. Willis, (London: University College), p. 232.
Clavel, J. 1983, preprint.
Collin-Souffrin, S., Joly, M., Heidmann, N., and Dumont, S. 1979, *Astr. Ap.*, **72**, 293.
Davidson, K., and Netzer, H. 1979, *Rev. Mod. Phys.*, **51**, 715.
Ferland, G. J., and Netzer, H. 1979, *Ap. J.*, **229**, 274.
Gahm, G. F. 1974, *Astr. Ap. Suppl.*, **18**, 259.
Grandi, S. A. 1981, *Ap. J.*, **251**, 451.
Johansson, S. 1977, *M.N.R.A.S.*, **178**, 17 p.
_____. 1978*a*, *Phys. Scripta*, **18**, 217.
_____. 1978*b*, *M.N.R.A.S.*, **184**, 593.
Joly, M. 1981, *Astr. Ap.*, **102**, 321.
Kurucz, R. L. 1981, *Smithsonian Astr. Obs. Spec. Rept.*, No. 390.
Kwan, J., and Krolik, J. H. 1981, *Ap. J.*, **250**, 478.
Moity, J. 1983, *Astr. Ap. Suppl.*, **52**, 37.
Moore, C. E. 1945, *A Multiplet Table of Astrophysical Interest* (*Princeton Univ. Obs. Contr.* No. 20).
_____. 1950, *An Ultraviolet Multiplet Table*, *NBS Circ.* 488.
Netzer, H. 1980, *Ap. J.*, **236**, 406 (Paper I).
Nussbaumer, H., Pettini, M., and Storey, P. J. 1981, *Astr. Ap.*, **102**, 351.
Nussbaumer, H., and Schild, H. 1981, *Astr. Ap.*, **101**, 118.
Nussbaumer, H. and Storey, P. J. 1980, *Astr. Ap.*, **89**, 308.
Oke, J. B., and Lauer, T. R. 1979, *Ap. J.*, **230**, 360.
Osterbrock, D. E. 1977, *Ap. J.*, **215**, 733.
Penston, M. V., *et al.* 1983, *M.N.R.A.S.*, **202**, 833.
Phillips, M. M. 1978*a*, *Ap. J. Suppl.*, **38**, 187.
_____. 1978*b*, *Ap. J.*, **226**, 736.
_____. 1979, *Ap. J. Suppl.*, **39**, 377.
Puetter, R. C. 1983, preprint.
Thackeray, A. D. 1977, Mem. *R.A.S.*, **83**, 1.
van der Hucht, K. A., Stencel, R. E., Haisch, B. M., and Kondo, Y. 1978, *Astr. Ap.*, **36**, 377.
Wampler, E. J., and Oke, J. B. 1967, *Ap. J.*, **148**, 695.
Wills, B. J., Netzer, H., Uomoto, A. K., and Wills, D. 1980, *Ap. J.*, **237**, 319 (Paper II).
Wills, B. J., Netzer, H., and Wills, D. 1980, *Ap. J.* (*Letters*), **242**, L1 (Paper III).

HAGAI NETZER: Department of Physics and Astronomy, Tel Aviv University, Ramat Aviv, Tel Aviv 69978, Israel

BEVERLEY J. WILLS: Department of Astronomy, RLM 15.220, University of Texas, Austin, TX 78712